Polar orientation induced by local photo-assisted poling in azo copolymer films

F. S.-S. Chien,[1,*] C. Y. Lin,[2,1] C. R. Huang,[1] C. S. Chang,[2] and C. C. Hsu[3]

[1]*Department of Physics, Tunghai University, Taichung, Taiwan*
[2]*Department of Photonics and Institute of Electro-Optical Engineering, National Chiao Tung University, Hsinchu 300, Taiwan*
[3]*Department of Physics, National Chung-Cheng University, Chiayi, Taiwan*
[*]*Corresponding author: fsschien@thu.edu.tw*

Received October 5, 2009; revised January 27, 2010; accepted February 8, 2010; posted February 16, 2010 (Doc. ID 118182); published March 31, 2010

Polar orientation created by local photo-assisted poling (PAP) in copolymer films containing disperse red 1 was investigated by scanning probe microscopy. PAP was performed by a proximal biased probe, and the polar orientation was semiquantitatively measured by electrostatic force microscopy. The polar orientation behaves as a biexponential function of the period of PAP, which is dominated by fast angular hole burning and slow angular redistribution (AR). The characteristic time of AR decreases linearly with the poling bias. An expression has been developed to interpret the evolution of the Lorentzian-like shape of the poled spots. A poled spot with 150 nm FWHM was demonstrated. © 2010 Optical Society of America

OCIS codes: 160.5320, 160.5470, 180.5810, 210.1635.

1. INTRODUCTION

Optical engineering of photoreactive polymers provides an efficient and convenient approach to generate nonlinear configuration for information storage [1,2] and second-harmonic generation (SHG) [3]. Maeda *et al.* [4] have demonstrated polarization storage in the guest-host polymethylmethacrylate (PMMA) thin film containing disperse red 1 (DR1). The DR1, azo-benzene molecule is a nonlinear optical chromophore that is well known for the *trans*↔*cis* photoisomerization excited by light [5]. The data bits were written by photoinduced orientation (PIO), which is activated by two-photon absorption (TPA) and read by confocal laser scanning microscopy in reflection mode.

Zyss's group [6] developed a new scheme for nonlinear optical memories. The data bits were written by all-optical poling (AOP) and read by the SHG response of the nonlinear chromophores in polymer films. The spatial resolution of the polar orientation is significantly improved to the submicron scale, due to conditions in which the nonlinear processes (AOP and SHG) are confined in the vicinity of the focal point (a volume of order λ^3, where λ is the laser wavelength). Dorkenoo's group [7] and Hsu's group [8] separately proposed another new approach, in which uniform orientation of a DR1-PMMA copolymer film was created by corona poling and the data bits were produced by the disorientation of the DR1 chromophores through TPA-induced photoisomerization. The data can be erased by heating the copolymer film and rewritten again after repoling the film. Consequently, rewritable optical storage is accomplished.

However, the spatial resolution of the typical optical-based methods, such as nonlinear optical measurements [7,8] and attenuated total reflection [9], is restricted by optical diffraction. To enhance the density of information storage in polymer films, some novel approaches based on scanning probe microscopy (SPM) have been demonstrated. For instance, protrusions with a diameter of 50 nm were produced by metal-probe-enhanced near-field illumination [10]. Also, submicron-scale polar orientation in azo polymer films was generated by probe-induced local photo-assisted poling (PAP) [11] in which a biased proximal probe provides an intense electric field to the azo polymer films under illumination. The polarization ($\vec{P}$) was analyzed *in-situ* by electrostatic force microscopy (EFM) [12], which detects the Coulomb force $F_C = -\sigma_b \cdot \vec{E}$ acting on the probe, where σ_b ($=\vec{P}\cdot\hat{n}$, $\hat{n}$: the surface normal unit vector) stands for the surface bound charges and $\vec{E}$ the electric field. Not only does it give a higher resolution than other optical detection methods, EFM can also investigate without disturbance to the orientation. In this work, we studied the kinetics of the polarization generated by probe-based PAP. The polarization behaves as a biexponential function of the period of PAP, and the reaction is governed by the fast angular hole burning (AHB) and the slow angular redistribution (AR). An analytical expression is introduced to interpret the evolution of the Lorentzian-like shape of the poled spot.

2. EXPERIMENT

DR1-PMMA copolymer was dissolved in chloroform, filtered with a 250 nm filter, and spin-coated on a cleaned conducting indium tin oxide (ITO) glass plate. The ITO glass served as the bottom electrode. The film was then subjected to post-baking at 80 °C for 1 hour to form a film with a thickness of about 0.1 μm. The film exhibited an absorption band ranging from 400 nm to 600 nm, with an absorption peak at 470 nm. A SPM was utilized to map

the topography, perform local PAP, and analyze the polarization of the film. The probe was metallic-coated and had a nominal force constant of 2 N/m and resonant frequency (f_0) of 75 kHz. EFM mapping was accomplished by a double-path scheme. To observe the variation of polarization quantitatively over the surface, the phase shift ($\Delta\phi$) of the oscillating cantilevers was measured during the second path while the probe was biased at +3 V and lifted by 30 nm.

For implementation of local PAP, a poling bias (V) was applied to the probe and a linearly polarized diode-pumped solid-state laser was used to stimulate the *trans*⇔*cis* photoisomerization, so that the *cis*-chromophores are free to be rotated at room temperature by the torque ($\vec{\mu}_c \times \vec{E}$, μ_c: dipole moment of *cis*-chromophores,). The wavelength and the beam diameter of the laser were 473 nm and 3 mm, respectively. The laser was not focused, so we assumed the laser light is a plane wave with a horizontal polarization (perpendicular to the applied dc electric field). This configuration makes PAP more efficient. To avoid contact electrification (charge transfer) between the probe and the copolymer, the SPM was operated in tapping mode to reduce the period of physical contact during poling [11].

3. RESULTS AND DISCUSSION

A. Semiquantitative Measurement of EFM

The cantilever was stimulated with a fixed frequency near f_0. The additional force F_C associated with the polar orientation of the film introduces shifts in the resonance frequency (Δf_0) and phase ($\Delta\phi$). Within a small shift limit, the relationships $\Delta f_0 \propto \partial F_C/\partial z \propto P \cdot \partial E/\partial z$ are true [13]. Near f_0, $\Delta\phi$ responds almost linearly to the shift of resonance frequency ($\Delta\phi \propto \Delta f_0$), and the phase shift is proportional to the polarization ($\Delta\phi \propto P$) under a fixed applied E field, because of the high quality factor (>300) of the cantilever.

To validate the semiquantitative measurement of EFM, an external dc bias was applied to the probe to mimic the effect of F_C and to verify the relation $\Delta\phi \propto \partial F_C/\partial z$. Since the dc bias induces a capacitive force ($F_B = -\frac{1}{2}\partial C/\partial z V^2$), $\Delta\phi$ should obey the relation $\Delta\phi \propto -\frac{1}{2}\partial^2 C/\partial z^2 V^2$. As shown in Fig. 1, $\Delta\phi$ demonstrates a quadratic function of V, and thus assures the capability of EFM for semiquantitative measurement of polarization.

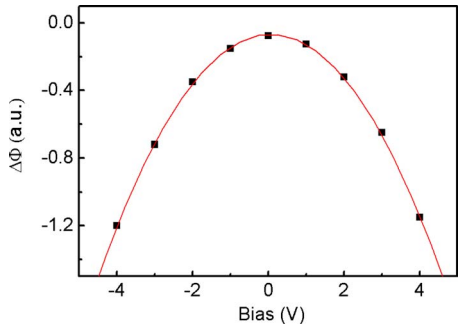

Fig. 1. (Color online) Phase shift ($\Delta\phi$) of an oscillating cantilever as a function of the bias.

B. Polarization *vs.* Laser Power

The film was subjected to a bias of +10 V and a laser power (P_L) of 500 μW for 360 s to achieve local PAP, while the oscillating probe was held still over the surface. The period of PAP (t) was equivalent to the time during which both the bias and laser were applied. The topographic and the EFM images were taken simultaneously, as shown in Figs. 2(a) and 2(b). The cross-sectional profile of the EFM image in Fig. 2(c) shows that the polarization is characterized by a Lorentzian-like shape. No plasmonic effect was produced to amplify the light at the probe apex, because there is no component with vertical laser polarization. Therefore, in Fig. 2(a), no remarkable change appears to the topography due to mass transport after PAP. Analytical expressions for nonlocal PAP-induced polarization based on a phenomenological theory have been presented [13]. Based on the theory, the polarization is associated with the molecular orientation as $\vec{P}(t) = N\mu_t 3T_1(t)/5\hat{z}$, where N is the molecular density of DR1 and $T_1(t)$ the first-order coefficient of the non-normalized Legendre expansion for the molecular angular distribution [14,15]. We assume that the contribution of *cis*-chromophores to the polarization is negligible. The peak of the induced polarization $P_p(t)$ as a function of t was studied under the illumination of various laser powers (10, 80, and 550 μW) and a fixed bias (−10 V). As shown in Fig. 3(a), $P_p(t)$ grows as a biexponential function of t [16], described by the following equation:

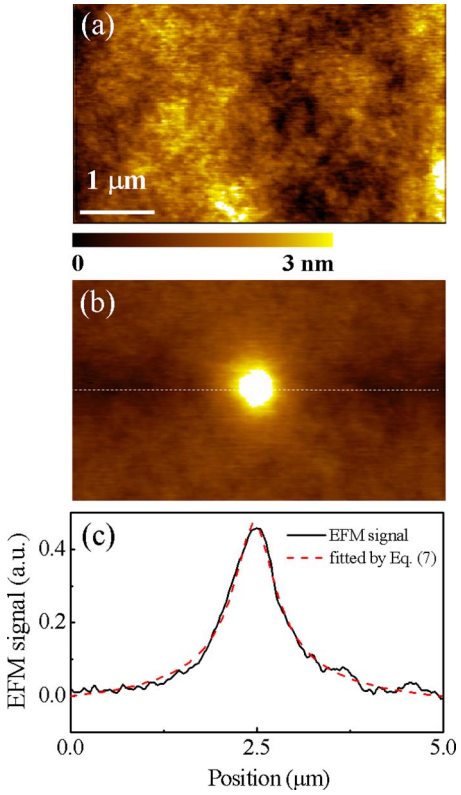

Fig. 2. (Color online) (a) and (b) Topographic and EFM images of a poled spot induced by local PAP on a DR1-PMMA copolymer film. (c) The profile of the EFM signal along the dashed line in (b).

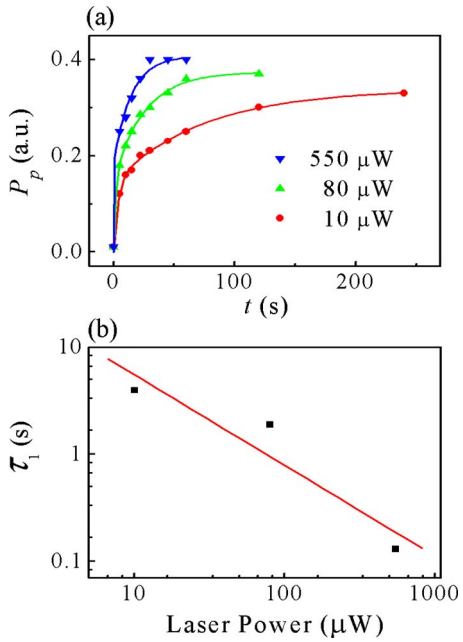

Fig. 3. (Color online) (a) Peak of the polarization (P_p) versus the period of local PAP (t) under various laser powers. (b) Plot of the characteristic time τ_1 as a function of laser power (P_L).

$$P_p(t) = P_0[1 - a_1 \exp(-t/\tau_1) - a_2 \exp(-t/\tau_2)], \qquad (1)$$

where P_0 is the saturated polarization, τ_1 and τ_2 are the response times of the chromophores to PAP, and a_1 and a_2 are coefficients of the exponential terms. The parameters were fitted according to Eq. (1), with the resulting values listed in Table 1. Note that P_0 is a function of the bias and laser power, and $a_1+a_2 \cong 1$.

The buildup of the polar orientation is associated with two reactions; namely, the fast AHB and slow AR [14,16]. AHB involves the *trans*→*cis* transition by optical pumping, and it results in an increase in the population of *cis* state. Contrarily, AR involves the orientation diffusion of the *cis* chromophores driven by the torque and the thermal agitation. Therefore, τ_i and a_i ($i=1,2$) can be regarded as the characteristic time and the weight of the reactions of AHB and AR. It is believed that, in the presence of an intense electric field, most molecules preserve the memory of orientation during the back-isomerization.

According to the values of the fitted parameters (Table 1), τ_1 and τ_2 behave differently in response to the laser power, and τ_1 is a few orders of magnitude shorter than τ_2. Note that τ_1 is inversely proportional to the laser power ($\propto P_L^{-1}$) as shown in Fig. 3(b), while τ_2 is less sensitive to P_L. We consider τ_1 to be the characteristic time of the *trans*→*cis* transition (also referred to as *pumping time*), since the pumping time is proportional to $(\sigma_t \Phi_{tc} P_L)^{-1}$, with σ_t representing the cross section for the absorption of one photon by a *trans*-chromophore, and Φ_{tc} the quantum yield of *trans*→*cis* photoisomerization [13]. Also, P_0 increases with P_L, because a high P_L gives a higher population of the rotatable *cis*-molecules.

Table 1. Values of the Fitted Parameters in Eq. (1) under Various Laser Powers

I (μW)	τ_1 (s)	τ_2 (s)	a_1	a_2	P_0
10	4.0	75	0.38	0.56	0.34
80	1.9	25	0.38	0.59	0.37
550	0.13	16	0.39	0.58	0.43

C. Polarization *vs.* Bias

We also analyzed $P_p(t)$ induced under various biases V (−2 V, −5 V, and −10 V) with a constant laser power exposure (100 μW). As illustrated in Fig. 4(a), $P_p(t)$ still obeys the biexponential behavior, and the values of the fitted parameters (P_0, τ_1, τ_2, a_1, and a_2) are listed in Table 2. τ_1 essentially remains constant (~2.9 s), having no apparent correlation with the bias because the *trans*→*cis* transition does not react to the bias. However, τ_2 decreases linearly with the bias as shown in Fig. 4(b). Therefore, we consider τ_2 as the angular diffusion time of AR under the poling electric field. Apparently τ_2 decreases with $|V|$ and thus is modified as

$$\tau_2 = \tau_D^c - \beta|V|, \qquad (2)$$

where τ_D^c=37.5 s is the onset of angular diffusion time for the *cis* state due to thermal effect, and β=2.9 is a proportionality coefficient that depends on the condition of the probe. The torque ($\vec{\mu}_c \times \vec{E}$) accelerates the angular diffusion of the chromophores to a specific direction, so the angular diffusion time should be associated with the bias.

According to the theory in [12], the angular diffusion is attributed to the thermal agitation of Brownian motion. The angular diffusion time is expressed as $\tau_D^c \propto \xi/kT$, where ξ, k, and T denote the viscosity of the *cis*-chromophores, the Boltzmann constant, and the absolute temperature, respectively. The electric field E is not directly involved with τ_D^c but appears as a prefactor in the expression of $T_1(t)$ (Eqs. 22 and 24 in Ref. [14]). The polar orientation increases with the strength of poling dc E

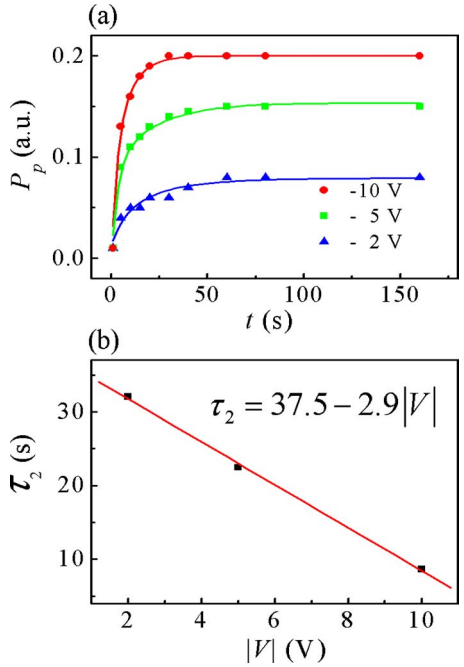

Fig. 4. (Color online) (a) P_p versus t under various poling biases. (b) Plot of the characteristic time τ_2 as a function of the bias.

Table 2. Values of the Fitted Parameters in Eq. (1) under Various Biases

Bias (V)	τ_1 (s)	τ_2 (s)	a_1	a_2	P_0
−2	2.9	32	0.56	0.50	0.08
−5	3.3	22	0.41	0.62	0.15
−10	2.8	8	0.50	0.50	0.20

field. Effectively, the angular diffusion time decreases with E, which is consistent with our observation.

It has been predicted that P_0 increases with the poling field [14]. As illustrated in Fig. 5, we observed the empirical dependence of P_0 on the bias in a square-root relation, given as $P_0(V)=\alpha\sqrt{|V|-V_0}$ ($\alpha=0.07$ is a constant and $V_o=0.97$ V is the threshold bias). The polarization was not detectable as the bias fell below the threshold bias V_o. The threshold bias depends on the film thickness and the probe condition. Based on this relationship, Eq. (1) can be rewritten as

$$P_p(V,t)=P_0(V)\left[1-a_1\exp\left(\frac{-t}{\tau_1}\right)-a_2\exp\left(\frac{-t}{\tau_D^c-\beta|V|}\right)\right]. \tag{3}$$

$P_p(V,t)$ is an explicit function of bias. As we take into account the distribution of the electric field, Eq. (3) can be modified to describe the Lorentzian-like shape of P. We propose that the poling electric field under the probe is represented by $V\cdot L(\rho,\sigma)$, where $L(\rho,\sigma)=\sigma^2/4\rho^2+\sigma^2$ is the Lorentzian function of radial distance ρ, and σ stands for the half width. The Lorentzian field could result from the geometry of the probe. Taking the field distribution into account, the polarization can be expressed as

$$P(\rho,V,t)=P_0(V,\rho)\left[1-a_1\exp\left(\frac{-t}{\tau_1}\right)-a_2\exp\left(\frac{-t}{\tau_D^c-\beta|V|\cdot L(\rho,\sigma)}\right)\right], \tag{4}$$

where $P_0(V,\rho)=\alpha\sqrt{|V|\cdot L(\rho,\sigma)-V_0}$ is the saturated polarization involving the field distribution. As $|V|\cdot L(\rho,\sigma)<V_o$, the effect of PAP is ignored. According to Eq. (4), we plotted the profile of PAP polarization with t, shown in Fig. 6, to simulate the evolution of the polarization with

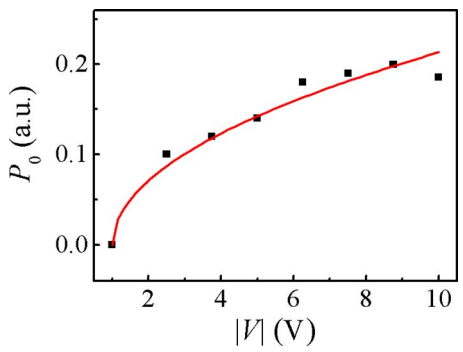

Fig. 5. (Color online) Plot of the saturated polarization (P_0) versus the poling bias.

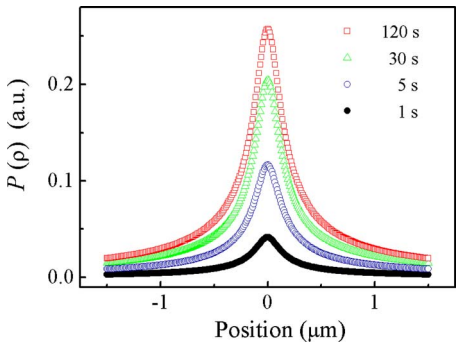

Fig. 6. (Color online) Evolution of the polarization profile $P(\rho)$ simulated by Eq. (4).

the following parameters: $V=-3$ V, $\tau_1=2.35$ s, $\tau_D^c=37.5$ s, $a_1=0.4$, $a_2=0.6$, $\sigma=235$ nm, $\alpha=0.15$, and $\beta=2.9$.

D. Evolution of the FWHM of Poled Spots

Because τ_2 varies with ρ, the polarization profile of the poled spots grows nonconformally. Therefore, the full width at half-maximum (FWHM) varies with t. Figure 7 shows the dependence of $P_p(t)$ and FWHM on t under a bias of −3 V and a laser power of 150 μW. It is evident that FWHM changes with t abnormally. Initially, FWHM decreases rapidly with t and reaches its minimum (370 nm) at ~30 s; then it increases slowly with t to reach the saturated point. The FWHM of the numerically derived profiles in Fig. 6 follows the same trends as shown in Fig. 7. Such a phenomenon can be understood through Eq. (4). In the beginning ($t\ll\tau_2$), Eq. (4) is approximated as

$$P(\rho,V,t)=P_0(V,\rho)\left[a_1\left(1-\exp\left(\frac{-t}{\tau_1}\right)\right)\right]. \tag{5}$$

During this period, the polarization is dominated by the fast AHB, and the FWHM is mainly determined by the width of P_0 (V,ρ). As t increases, AR begins to influence the growth of polarization. When $t\gg\tau_1$, Eq. (4) is approximated as

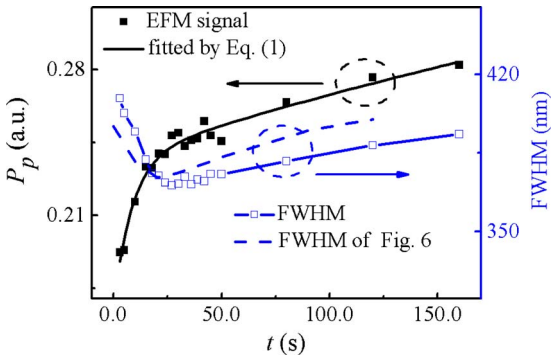

Fig. 7. (Color online) Evolution of P_p and FWHM of a poled spot created by −3 V bias and 150 μW laser, along with the FWHM predicted by Eq. (4). The FWHM of $P(\rho)$ in Fig. 6 is also shown (dashed curve).

$$P(\rho,V,t) = P_0(V,\rho)\left[1 - a_2 \exp\left(\frac{-t}{\tau_D^c - \beta|V| \cdot L(\rho,\sigma)}\right)\right]. \quad (6)$$

Under this circumstance, τ_2 increases with ρ, so AR presents a ρ-dependent enhancement to the growth of polarization. The enhancement of the AR-related factor decreases with ρ, i.e., $P(\rho=0,V,t)$ grows faster than the outer area. When $P(\rho=0,V,t)$ approaches its saturated point, the FWHM of $P(\rho V,t)$ reaches its minimum.

Afterward, the outer area around $\rho=0$ gradually reaches the saturated point, so FWMH increases with t until the poling effect terminates. Therefore when $t \gg \tau_2$, Eq. (6) becomes

$$P(\rho,V,t \gg \tau_2) \cong P_0(V,\rho), \quad (7)$$

, which suggests that the saturated FWHM should be close to the initial FWHM. The profile of the saturated polarization shown in Fig. 2 is well fitted by Eq. (7) ($\alpha=0.72$ and $\sigma=500$ nm) to demonstrate its validity.

There is a little discrepancy between the experimental and theoretical FWHMs in Fig. 7. We regard the major cause of the discrepancy to be the fact that the effect of the "vector" electric field was overestimated by the "scalar" Lorentzian potential field.

According to these analyses, the optimum period of PAP for generating minimum poled spots on the film was obtained. A poled spot of 150 nm FWHM was made by a fresh probe with $V=-3$ V and $t=30$ s, as shown in Fig. 8.

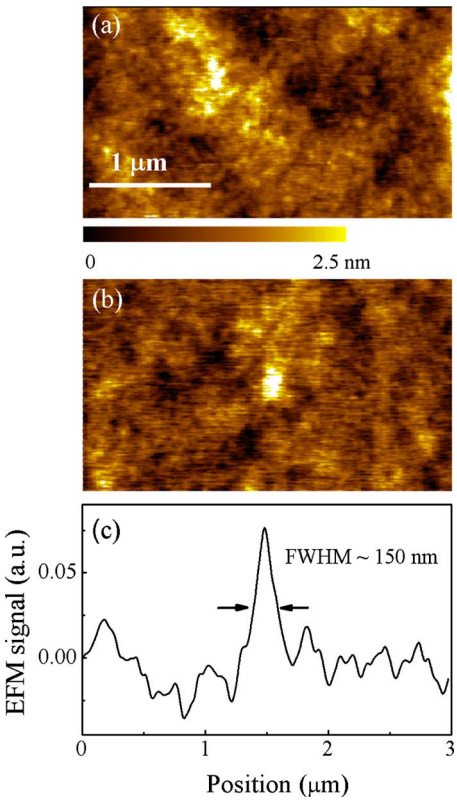

Fig. 8. (Color online) (a) and (b) Topographic and EFM images of a poled spot. (c) Profile of EFM signal along the center of the spot in (b) to show its FWHM (150 nm).

Such a size is well below those produced by other optical-induced orientation methods on photoreactive films.

The efficiency of the induced polar orientation is a major concern to the applications of photoreactive polymers. PAP is more efficient than the methods in which only optical photoinduced orientation is involved. Normally, τ_2 is much longer than τ_1, so the slow AR is the limiting process for inducing orientation. The efficiency can be improved as τ_2 is reduced by the E field in PAP; an estimate by Eq. (2) indicates that τ_2 can be reduced by 50% with a 20 V bias. In addition, the carrier-to-noise ratio is also improved by PAP, for P_0 is enhanced with the E field. It is worth noting that P_0 cannot be enhanced simply by the increase of the intensity of light [17], because the rates of *cis*→*trans* transition and the thermal angular diffusion increase as well. However, we did not observe any decrease of P_0, even as the laser power increased by two orders of magnitude. This result could be attributed to the decrease in τ_2 and the higher memory of the molecular alignment of *cis*→*trans* transition. Therefore, local PAP with scanning probes is an efficient method for the creation of polar orientation.

4. CONCLUSION

The polar orientation of local PAP in DR1-PMMA copolymer films was induced by scanning probes and investigated by EFM. The polar orientation obeys a biexponential function of the period of PAP. The kinetics is dominated by the characteristic times of AHB and AR. The poling field can effectively reduce the characteristic time of AR. An analytical expression depicting the Lorentzian-like shape of the poled spots was derived, and the evolutions of the polarization as well as the FWHM of the spots were interpreted. Local PAP is a more efficient approach than all-optical methods to generate subdiffraction-limit polar orientation. A poled spot of 150 nm FWHM was produced.

ACKNOWLEDGMENTS

The authors gratefully acknowledge the support of the National Science Council of Taiwan under grant NSC 96-2112-M-029-005-MY3.

REFERENCES

1. Z. Sekkat, J. Wood, W. Knoll, W. Volksen, R. D. Miller, and A. Knoesen, "Light-induced orientation in azo-polyimide polymers 325 °C below the glass transition temperature," J. Opt. Soc. Am. B **14**, 829–833 (1997).
2. N. Matsuoka, K. Kitaoka, J. Si, K. Fujita, and K. Hirao, "Second-order nonlinearity and optical image storage in phenyl-silica hybrid films doped with azo-dye chromophore using optical poling technique," Opt. Commun. **185**, 467–472 (2000).
3. G. Martin, S. Ducci, R. Hierle, D. Josse, and J. Zyss, "Quasi-phase matched second-harmonic generation from periodic optical randomization of poled polymer channel waveguides," Appl. Phys. Lett. **83**, 1086–1088 (2003).
4. M. Maeda, H. Ishitobi, Z. Sekkat, and S. Kawata, "Polarization storage by nonlinear orientational hole burning in azo dye-containing polymer films," Appl. Phys. Lett. **85**, 351–353 (2004).
5. Z. Sekkat, "Photo-orientation by photoisomerization," in

Photoreactive Organic Thin Films, Z. Sekkat and W. Knoll eds. (Academic, Elsevier Science, 2002), Chap. 3.
6. S. Bidault, J. Gouya, S. Brasselet, and J. Zyss, "Encoding multipolar polarization patterns by optical poling in polymers: towards nonlinear optical memories," Opt. Express **83**, 505–509 (2005).
7. D. Gindre, A. Boeglin, A. Fort, L. Mager, and K. D. Dorkenoo, "Rewritable optical data storage in azobenzene copolymers," Opt. Express **14**, 9896–9900 (2006).
8. J. H. Lin, N. D. Lai, C. H. Chiu, C.-Y. Lin, G. W. Rieger, J. F. Young, F. S.-S. Chien, and C. C. Hsu, "Fabrication of spatial modulated second order nonlinear structures and quasi-phase matched second harmonic generation in a poled azo-copolymer planar waveguide," Opt. Express **16**, 7832–7841 (2008).
9. Z. Sekkat, C.-S. Kang, E. F. Aust, G. Wegner, and W. Knoll, "Room-temperature photoinduced poling and thermal poling of a rigid main-chain polymer with polar azo dyes in the side chain," Chem. Mater. **7**, 142–147 (1995).
10. H. Ishitobi, M. Tanabe, Z. Sekkat, and S. Kawata, "Nano-movement of azo polymers induced by metal tip enhanced near-field irradiation," Appl. Phys. Lett. **91**, 091911 (2007).
11. F. S.-S. Chien, C. Y. Lin, and C. C. Hsu, "Local photo-assisted poling azo copolymer films by scanning probe microscopy," J. Phys. D: Appl. Phys. **41**, 235502 (2008).
12. D. Sarid, *Scanning Force Microscope: with applications to electric, magnetic, and atomic forces* (Oxford Univ. Press, 1991).
13. M. J. Gordon and T. Baron, "Amplitude-mode electrostatic force microscopy in UHV: quantification of nanocrystal charge storage," Phys. Rev. B **72**, 165420 (2005).
14. Z. Sekkat and W. Knoll, "Creation of second-order nonlinear optical effects by photoisomerization of polar azo dyes in polymeric films: theoretical study of steady-state and transient properties," J. Opt. Soc. Am. B **12**, 1855–1867 (1995).
15. G. Xu, X. Liu, J. Si, P. Ye, Z. Li, and Y. Shen, "Modified theory of photoinduced molecular polar alignment in azo polymers," Opt. Lett. **25**, 329–331 (2000).
16. C.-C. Hsu, J.-H. Lin, T.-H. Huang, and K. Harada, "Temperature-dependent photoinduced third-harmonic-generation variation in azo-homopolymer and azo-doped polymer thin films," Appl. Phys. Lett. **82**, 2440–2442 (2003).
17. M. Dumont, Z. Sekkat, R. Loucif-Saibi, K. Nakatani, and J. A. Delaire, "Photoisomerization, photo-induced orientation and orientational relaxation of azo dyes in polymeric films," Nonlinear Opt. **5**, 395 (1993).